Supporting Information

Multifunctional Smart Yolk-Shell Nanostructure with Mesoporous MnO_2 Shell for Enhanced Cancer Therapy

Hongjun Zhuang,[†] Mengyao Zhao,[†] Shenglong Ding,[‡] Lingyan Liu,[†] Wei Yuan,[†] Liping Jiang,[§] Xuemin Han,[£] Libo Jiang[*‡] and Tao Yi[*†£]

[†]Department of Chemistry, Fudan University, Shanghai 200438, P. R. China
[‡]Department of Orthopaedic Surgery, Zhongshan Hospital, Fudan University, Shanghai 200032, P. R. China
[§]Department of Macromolecular Science, Fudan University, Shanghai 200438, P. R. China
[£]College of Chemistry, Chemical Engineering and Biotechnology, Donghua University, Shanghai 201620, P. R. China

E-mail: jiang.libo@zs-hospital.sh.cn; yitao@fudan.edu.cn

Content

1. Experiment Section.....S-2
1.1 Chemicals and Materials.....S-2
1.2 Synthesis S-2
1.3 Characterization..... S-4
2. Additional figures S-5
3. Additional tables.....S-25
4. References.....S-26

1. Experimental section

1.1 Chemicals and Materials. Erbium (III) chloride hexahydrate (99.9%), yttrium (III) chloride hexahydrate (99.9%), sodium trifluoroacetate (Na-TFA, 98 %), 1-octadecene (ODE, 90%), oleic acid (OA, 90%), 3–4,5-dimethylthiazol-2-yl-2,5-diphenyl tetrazolium bromide (MTT) and tetraethyl orthosilicate (TEOS) were purchased from Sigma-Aldrich (Shanghai, China). Sodium hydroxide (NaOH, 96%), ammonium fluoride (NH_4F, 96%), methanol, ethanol, 1-octanol, Triton X-100, Cyclohexane, $NH_3 \cdot H_2O$ (28 wt.%), Potassium permanganate ($KMnO_4$) and sodium carbonate (Na_2CO_3) were purchased from Sinopharm Chemical Reagent Co., Ltd. (China). Poly (allylamine hydrochloride) (PAH, MW~15,000), polyacrylic acid (PAA, MW~2000), mPEG-NH_2 (MW~5000), Hydrogen peroxide (H_2O_2, 30 wt%), 1-(3-Diaminopropyl)-3-ethylcarbodiimide hydrochloride (EDC·HCl, 98.5%), N-hydroxysuccinimide (NHS, 98%) and mPEG-NH_2 (MW = 5000) were purchased from Alfa Aesar Chemical Ltd. (Tianjin, China). 1,3-diphenylisobenzofuran (DPBF), 2′,7′-dichlorodihydrofluorescein diacetate (DCFH-DA), Doxorubicin Hydrochloride (DOX·HCl), Methylene blue (MB), 4',6-diamidino-2-phenylindole (DAPI) and trypan blue were purchased from J&K chemical Co., Ltd. (China). All chemicals formed receiving without any further purification.

1.2 Synthesis

1.2.1 Synthesis of β-$NaErF_4$ (UC) nanoparticles. The synthesis of UC with a size of ~ 18 nm in this work was according to previously reported procedure.[1] In a typical procedure, 1.00 mmol $ErCl_3$, 6.0 mL OA and 15.0 mL ODE were mixed together and heated to 130 °C under vacuum until a clear solution formed. After that, the solution was cooled to room temperature. A solution of 2.5 mmol NaOH and 4.0 mmol NH_4F in 10 mL methanol was added and the mixture was stirred for one hour. The reaction mixture was then heated at 80 °C to remove methanol. Then the solution was heated to 300 °C and maintained at that temperature for 60 min under a gentle argon flow. Subsequently, the solution was cooled down to room temperature and the UC was precipitated, centrifuged and washed twice with ethanol. UC was finally dispersed in 10 mL of cyclohexane for further use.

1.2.2 Preparation of β-$NaErF_4$@$NaYF_4$ (UCP) nanoparticles. The core-shell nanoparticles were fabricated by the one-pot successive layer-by-layer (SLBL) protocol.[2] 5 mL of the purified UC solution (~ 0.50 mmol) were mixed with 8.0 mL OA and 12.0 mL ODE. The flask was pumped

down at 70 °C for 30 min to remove cyclohexane, along with any residual air. Subsequently, the system was switched to Ar flow and the reaction mixture was further heated to 280 °C at a rate of ~ 15 °C min^{-1}. Then pairs of Y-OA (0.10 M, 15.0 mL) and Na-TFA-OA (0.40 M, 7.50 mL) precursors were alternately introduced by dropwise at a speed of 3.0 mL/h at 280 °C. Finally, the obtained UCP nanoparticles were washed with ethanol and dispersed in cyclohexane.

1.2.3 Synthesis of β-$NaErF_4$@$NaYF_4$@SiO_2 (UCS) nanoparticles. UCS nanoparticles were synthesized through inverse microemulsion method[3]. First and foremost, 6.7 mL octanol and 12 mL of triton X-100 were dispersed in 50 mL cyclohexane by stirring. Then, 1.0 mL 10 mg·mL^{-1} UCP cyclohexane solutions were added into the above mixture. The resultant solution was stirred for 15 min, then 0.4 mL 28 wt% ammonium hydroxide solution was in addition to form a reverse microemulsion solution. After stirring for 30 min, and 0.3 mL TEOS was added, then the resultant reaction aged for 24 h under stirring. The final products were obtained by centrifuging and washed by water and ethanol several times. The core-shell-shell UCS nanoparticles were finally dispersed in 10 mL water for additional coating of MnO_2 shell.

1.2.4 Synthesis of β-$NaErF_4$@$NaYF_4$@SiO_2@MnO_2 (UCSM) nanoparticles. The synthesis of the UCSM nanoparticles was referred to preceding synthesis report[4] with a slight change. First and foremost, 10 μM TEOS was added drop by drop into 2 mL 10 mM UCS and continuous stirred for 0.5 h. Then 30 mL 0.2 M $KMnO_4$ was dropwise added into the suspension of above solution under ultrasonication for 2 h. The obtained mesoporous UCSM was achieved by centrifuging and washing with water several times.

1.2.5 Synthesis of y-$NaErF_4$@$NaYF_4$@MnO_2-PEG (y-UCM-PEG) YSNs. The as-prepared mesoporous UCSM was dissolved in 0.5 M Na_2CO_3 aqueous solution at 60 °C for 0.5 h. The obtained y-UCM YSNs were centrifuged and washed with water several times. y-UCM-PEG were synthesized through layer-by-layer assembly (LBL) method. Overall, y-UCM solution was added into 40 mL 5 mg·mL^{-1} PAH solution under ultrasonication. After stirring for 2 h, the above solution was centrifuged and washed with water. The obtained y-UCM-PAH solution was added into 40 mL 5 mg·mL^{-1} PAA dropwise under ultrasonication. After 2 h of stirring, the above solution was centrifuged and washed with water. Then 20 mL 3 mg·mL^{-1} EDC and 20 mL 10 mg·mL^{-1} mPEG-NH_2 were added into the above solution and continuing to stir for 12 h. Finally, the prepared y-UCM-PEG was harvested by centrifugation and washed with water for three times.

1.3 Characterization. Transmission electron microscopy (TEM) images were performed using a Tecnai G2 20 TWIN transmission electron microscope with an accelerating voltage of 200 kV equipped with a post column Gatan imaging filter (GIF-Tri-dium). Field Emission Transmission Electron Microscope (FETEM) images were obtained using a Tecnai G2 F20 S-Twin with an accelerating voltage of 200 kV with X-Max 80T and Be4-Cf98 EDS. High contrast transmission electron microscopy (HCTEM) was performed using a Hitachi HT7800 transmission electron microscope with an accelerating voltage of 100 kV. Field emission scanning electron microscopy (FESEM) images were taken using a Zeiss Ultra 55. Absorption spectra were gathered by using a PerkinElmer Lambda 750S UV-visible-NIR spectrometer with a 600 nm min^{-1} scan rate and a Shimadzu UV-2600 spectrophotometer. The emission spectra were found on an Edinburgh Instrument FLS980 fluorescence spectrometer, but an external 980-nm semiconductor laser was used as the excitation source (Changchun New Industries Optoelectronics Tech. Co., Ltd.). With an optic fiber accessory, instead of Xeon source in the spectrophotometer (unless otherwise specified), all spectra were obtained under identical experimental conditions.

X-ray powder diffraction (XRD) pattern measurements were performed using a Bruker D4 diffractometer at a scanning rate of 1° min^{-1} in the 2θ range from 10° to 90° (Cu Kα radiation, λ = 0.15406 nm). FTIR spectra were obtained using a ThermoFisher Nicolet 6700 spectrometer from samples in KBr pellets. Zeta potentials were taken using a Malvern nanoparticle size-zeta potential analyzer. Nitrogen adsorption-desorption measurements were conducted at 77 K with ASAP 2420 and Micromeritcs Tristar 3020 analyzer (USA) to gather information on the porosity. Before measurements, the samples were degassed in vacuum at 120 °C for at least 12 h. Distribution of nanoprobes depended on measuring Er^{3+} content in different organs by inductively coupled plasma atomic emission spectrometry (ICP) using a ThermoFisher iCAP 7400 ICP-AES.

The NIR-II fluorescence *in vivo* imaging was performed with a modified home-built InGaAs array detector (Princeton Instruments, NIR vana 640), cooled down to -80 °C, the analog to digital conversion rate set to 10 MHz and exposure time set to 100 ms. 633-nm and 980-nm lasers were used as the excitation source, in combination with two long pass optical filters (1200 nm long-pass filter from thorlabs). 700 nm long-pass filter (Thorlabs) was utilized for collect MB fluorescence signal. Photoacoustic/ultrasonic imaging was performed using Vevo LAZR multi-mode photoacoustic/ultrasonic imaging system with YAG laser, optical parametric oscillator (OPO)

(FujiFilm VisualSonics Inc.). Confocal scanning laser microscope images were taken from IX81, (Olympus, Japan) with an external 980-nm semiconductor laser.

2. Additional Figures

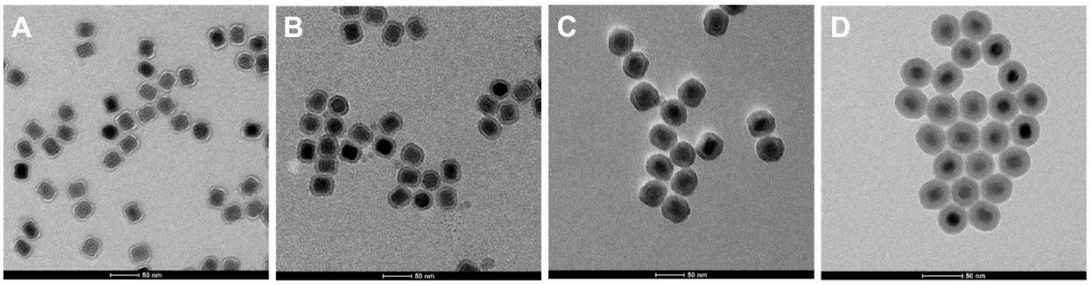

Figure S1. TEM images of UCS with different thickness of SiO_2, 2 nm (A), 5 nm (B), 8 nm (C), 10 nm (D).

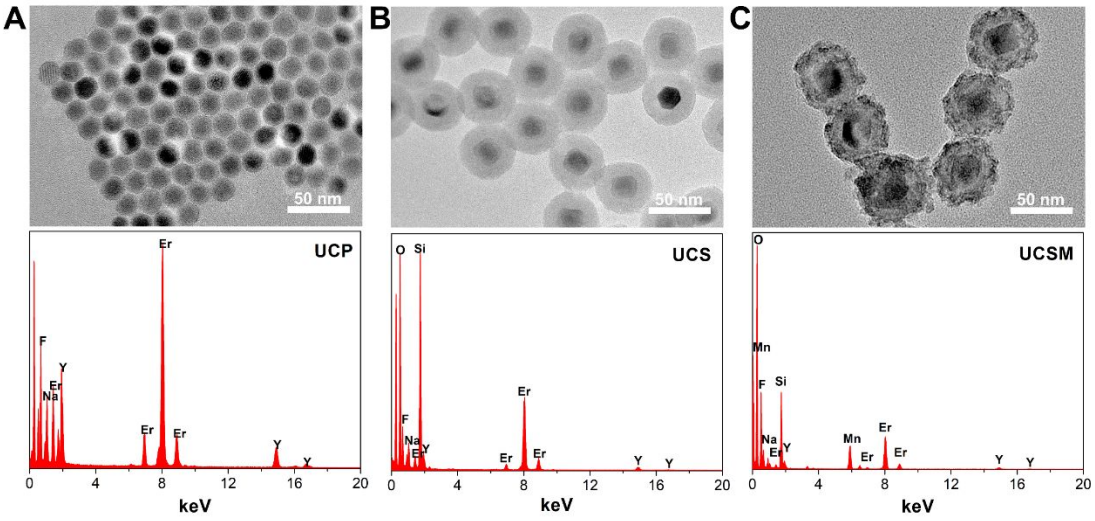

Figure S2. HRTEM images and EDS spectrums of UCP (A), UCS (B), UCSM (C).

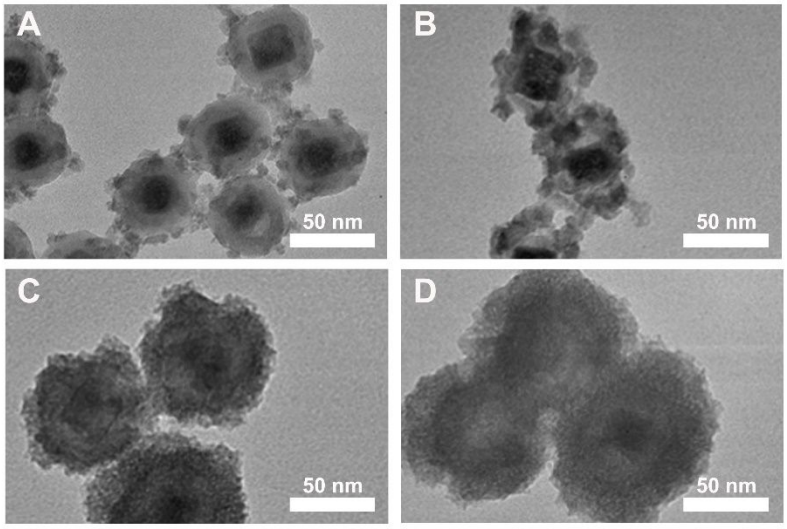

Figure S3. TEM images of UCSM at different concentrations of TEOS. (A) 0 μM, (B) 5 μM, (C) 10 μM and (D) 20 μM.

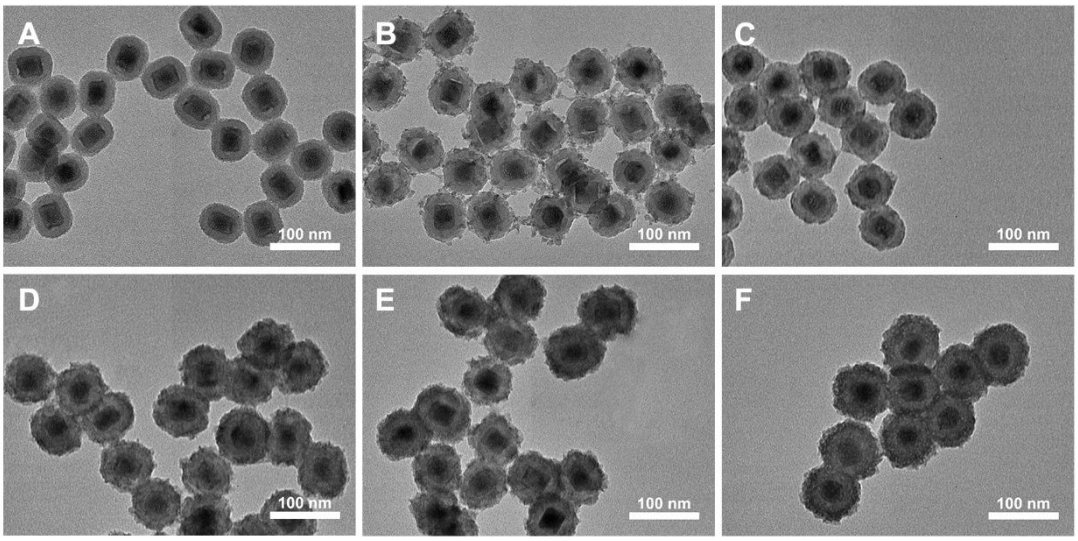

Figure S4. TEM images of UCSM with different thickness of MnO_2, (A) 0 nm, (B) 1 nm, (C) 3 nm, (D) 6 nm, (E) 9 nm and (F) 14 nm.

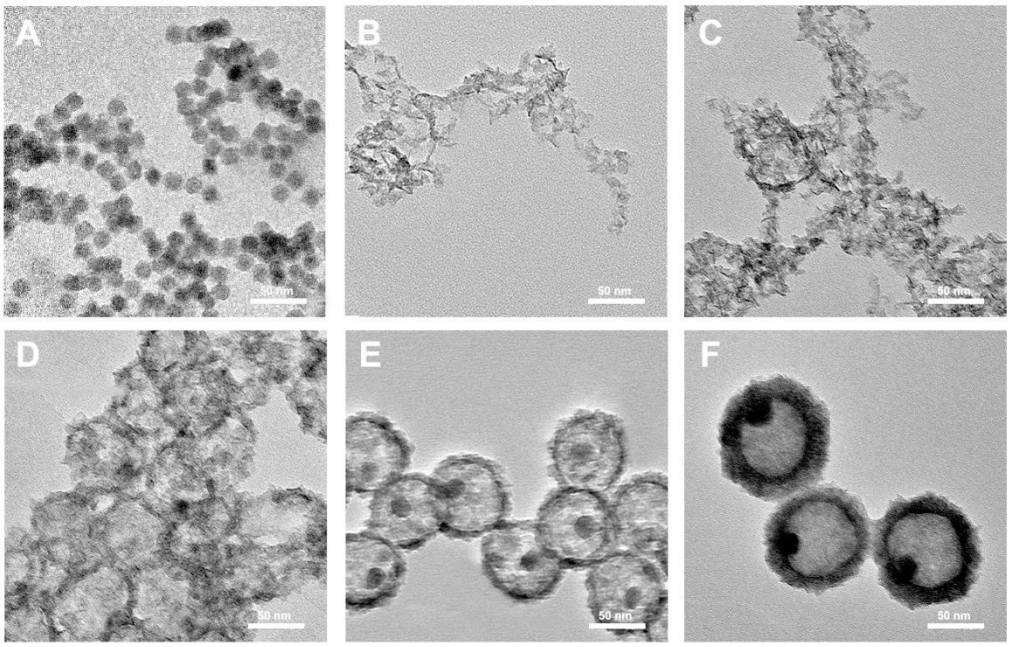

Figure S5. TEM images of y-UCM with different thickness of MnO_2, (A) 0 nm, (B) 1 nm, (C) 3 nm, (D) 6 nm, (E) 9 nm and (F) 14 nm.

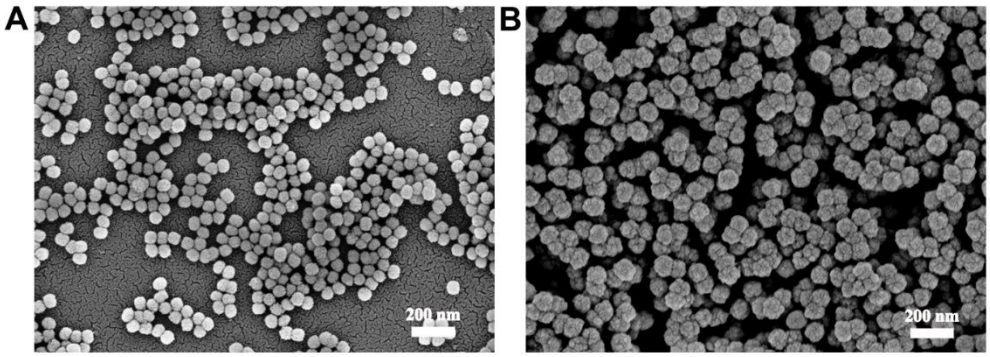

Figure S6. SEM images of UCS (A) and UCSM (B).

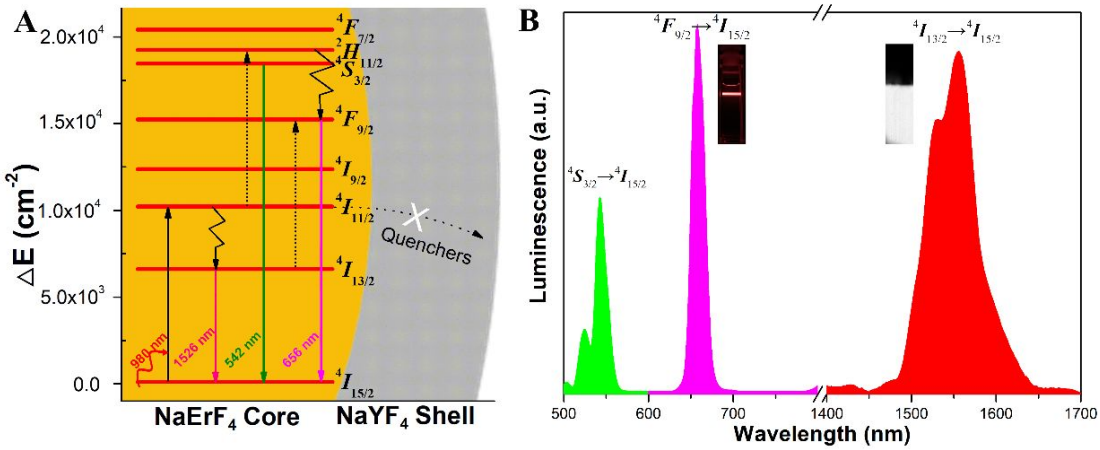

Figure S7. (A) Energy transfer mechanism of UCP nanoparticles. (B) Upconversion emission spectrum of UCP in the visible region (450−850 nm) with 980-nm laser excitation (0.5 W·cm^{-2}). Inset: digital photograph of the upconverted red emission from a cyclohexane dispersion of y-UCM.

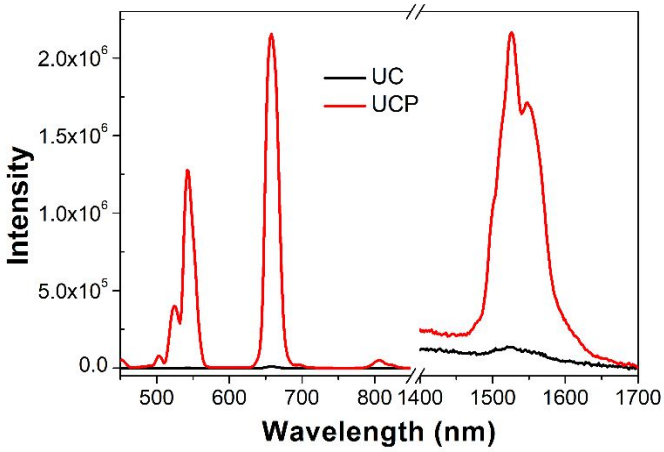

Figure S8. Fluorescence emission spectra of UC and UCP under excitation of 980-nm laser (P = 0.5 W·cm^{-2}). Concentration was 1.0 mM.

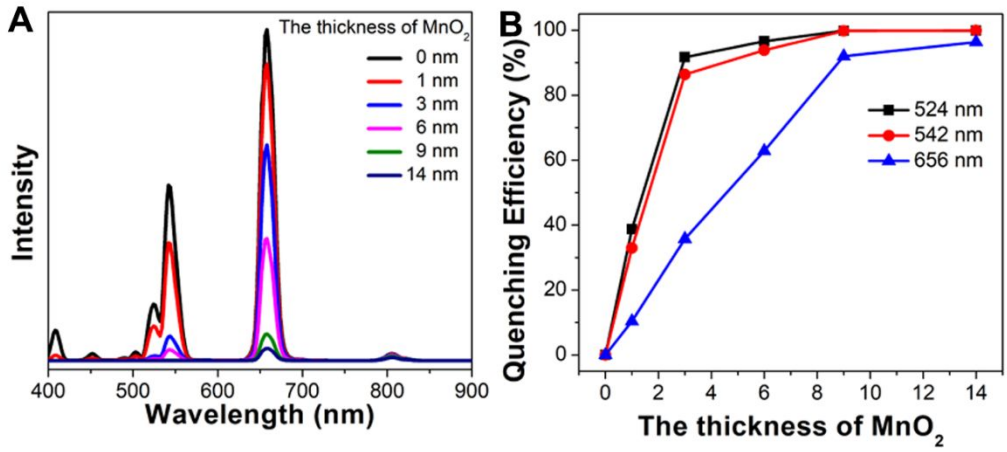

Figure S9. (A) Upconversion emission spectra of UCSM with different thickness of MnO_2. (B) Plot of luminescence intensity at 524, 542 and 656 nm against the thickness of MnO_2. The spectra were recorded under excitation of 980-nm laser at a power density of 0.5 $W \cdot cm^{-2}$. Concentration was 1.0 mM.

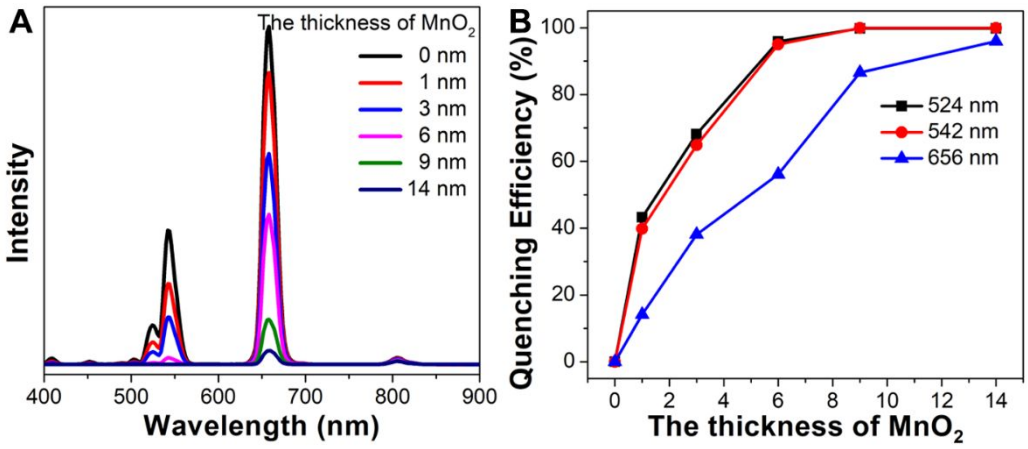

Figure S10. (A) Upconversion emission spectra of y-UCM with different thickness of MnO_2. (B) Plot of luminescence intensity at 524, 542, and 656 nm against the thickness of MnO_2. The spectra were recorded under excitation of 980-nm laser at a power density of 0.5 $W \cdot cm^{-2}$. Concentration was 1.0 mM.

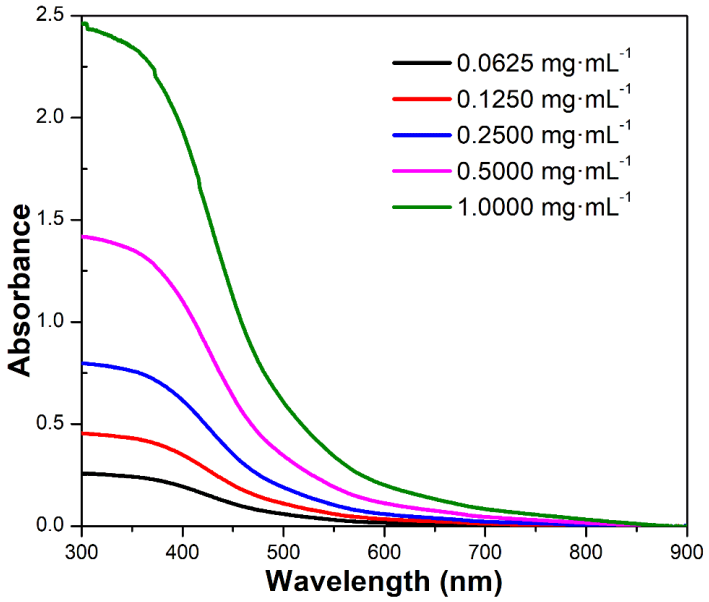

Figure S11. UV–vis absorption spectra of different concentrations of y-UCM-PEG.

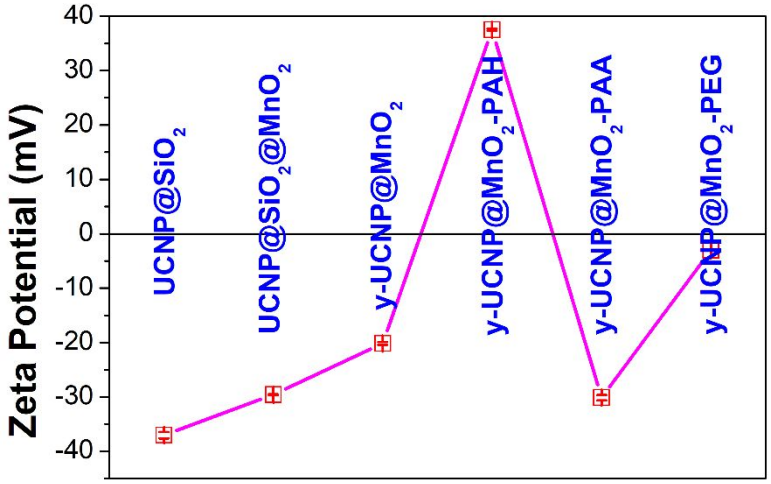

Figure S12. The changes of zeta potentials for nanoparticles obtained at different steps of fabrication (n = 3).

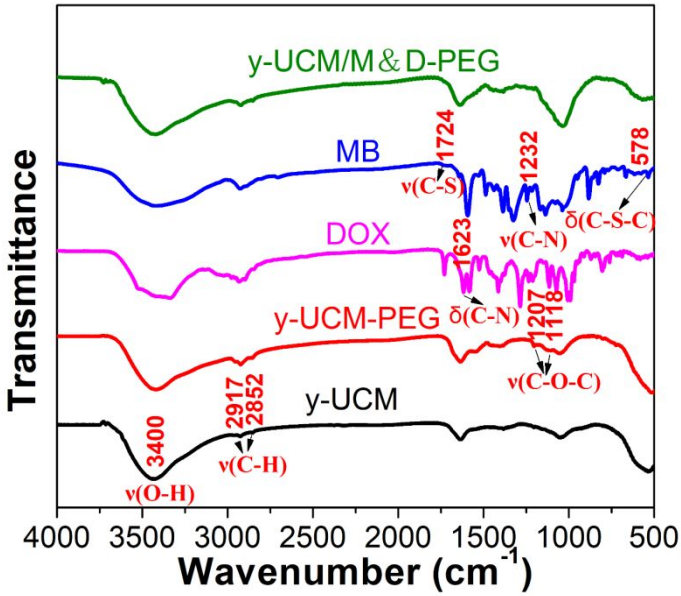

Figure S13. FT-IR spectra of y-UCM, y-UCM-PEG, DOX, MB and y-UCM/ M&D-PEG.

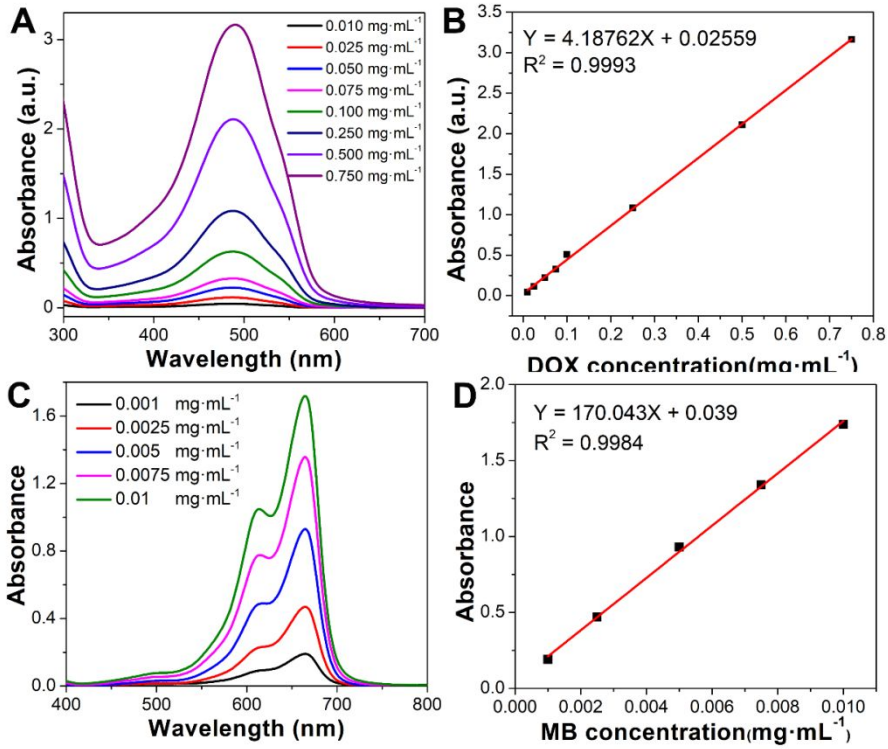

Figure S14. The standard curves for (A, B) DOX solution detected at 480 nm (Y = 16.78323X + 0.02325) and (C, D) MB solution detected at 664 nm (Y = 170.043X+0.039, R^2 = 0.9984), respectively.

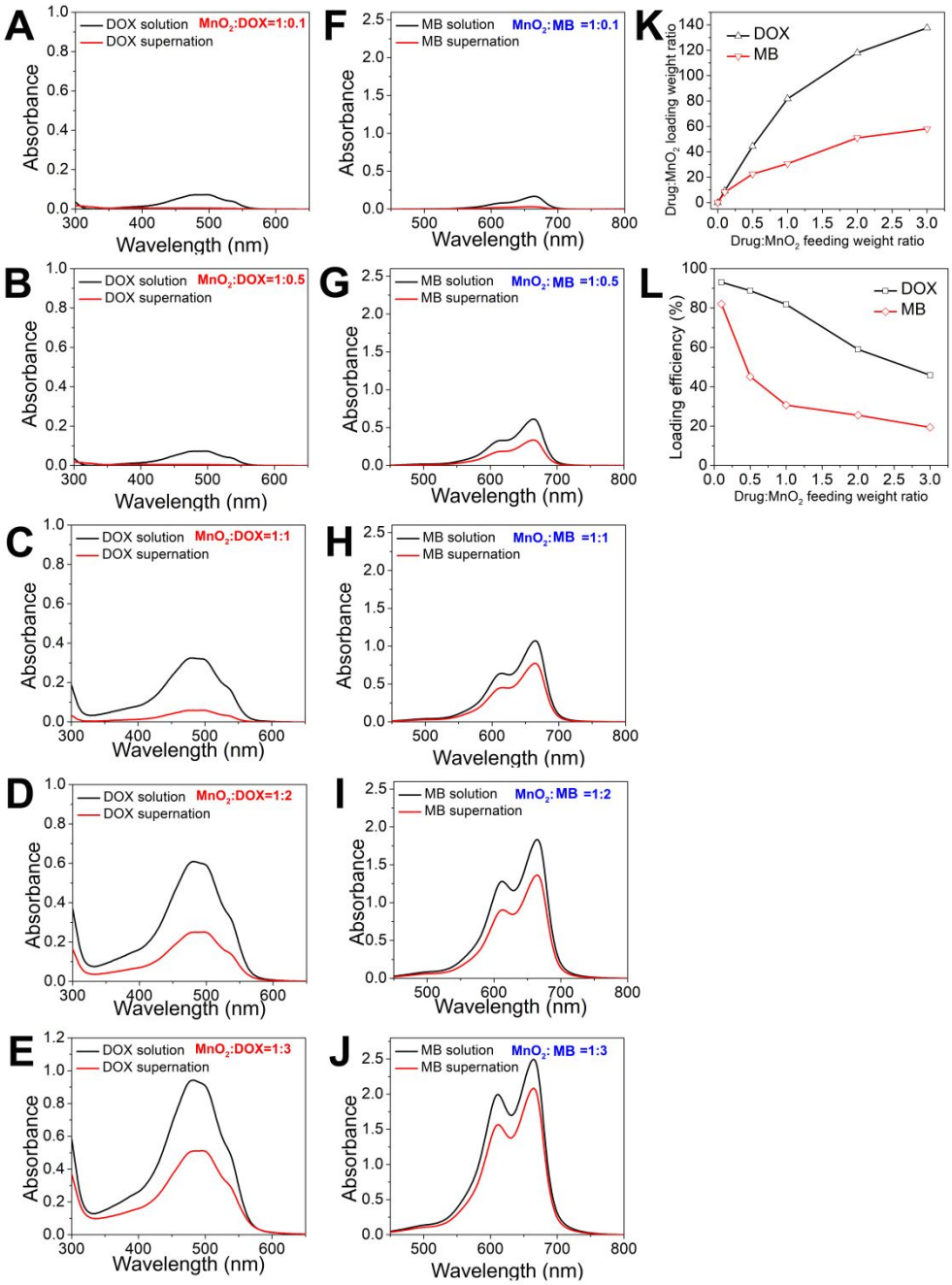

Figure S15. The absorption spectra of the initial DOX solution and the supernatant obtained with different DOX: MnO_2 loading weight ratios of (A) 1: 0.1, (B) 1: 0.5, (C) 1: 1, (D) 1: 2, (E) 1: 3; the absorption spectra of the initial MB solution and the supernatant obtained with different MB: MnO_2 loading weight ratios of (F)1: 0.1, (G) 1: 0.5, (H) 1: 1, (I) 1: 2, (J) 1: 3; drugs (DOX, MB): MnO_2 loading weight ratios (K) and loading efficiency (L) with different feeding weight ratios.

$$loading\ efficiency\ \ (\%)\ = \frac{\text{feeding weight of drug} - \text{weight of drug in supernatant}}{\text{feeding weight of drug}} \times 100$$

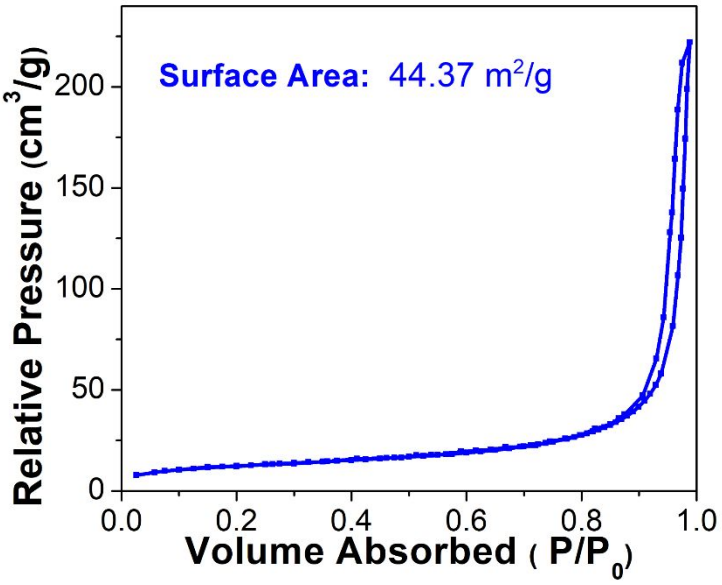

Figure S16. N_2 absorption-desorption isotherm of UCSM.

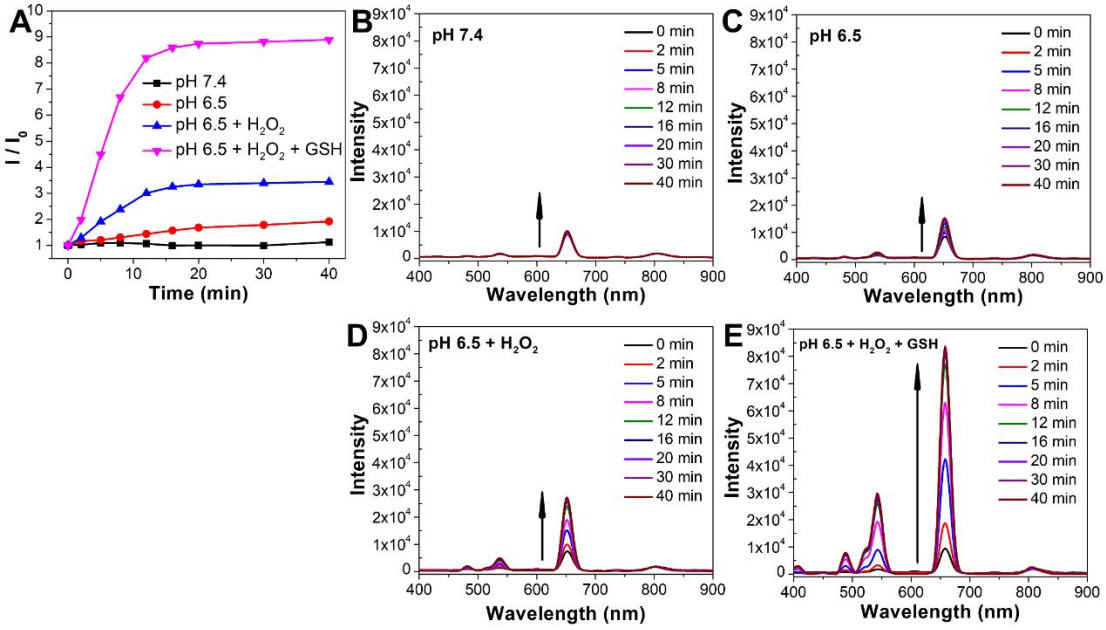

Figure S17. (A) The ratio of fluorescence intensity (I/I_0) at 656 nm and (B-E) the corresponding fluorescent spectral changes of y-UCM-PEG over time in different conditions under excitation of 980 nm laser. Concentration was 1.0 mM.

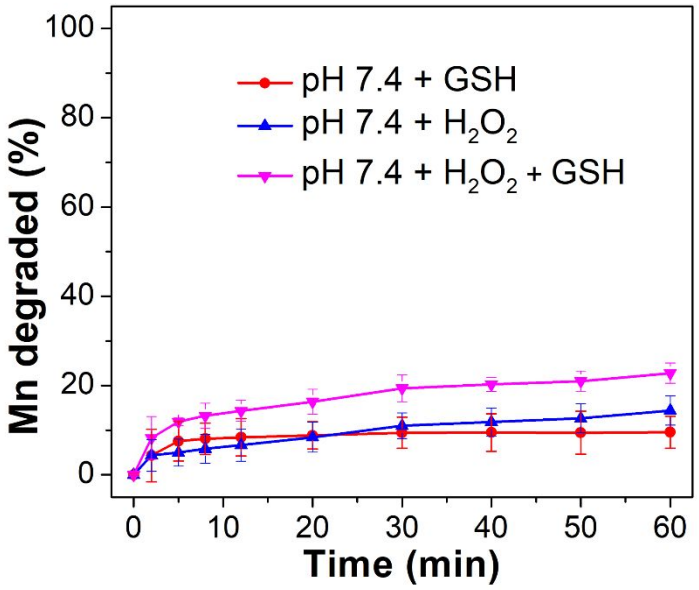

Figure S18. Percentages of accumulated release profiles of Mn^{2+} from y-UCM-PEG over time in different conditions (n = 3).

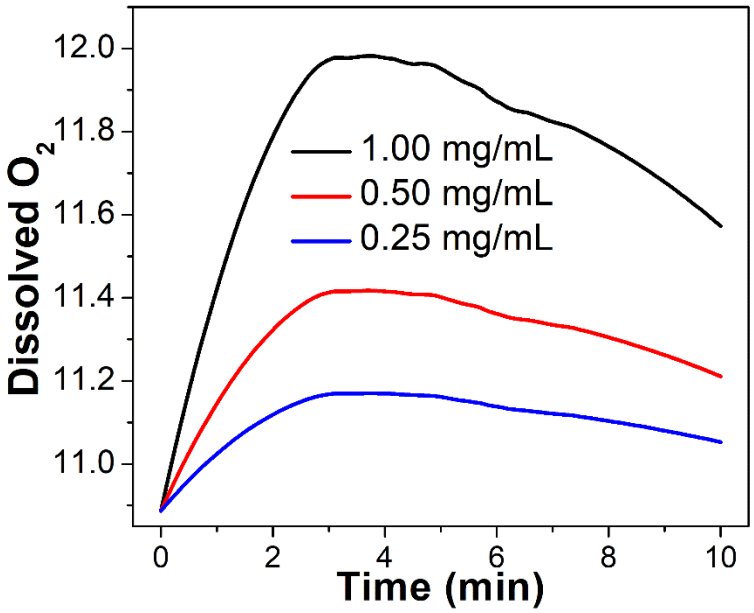

Figure S19. The concentration of O_2 produced from various concentrations of y-UCM/M&D-PEG in simulated TME solution.

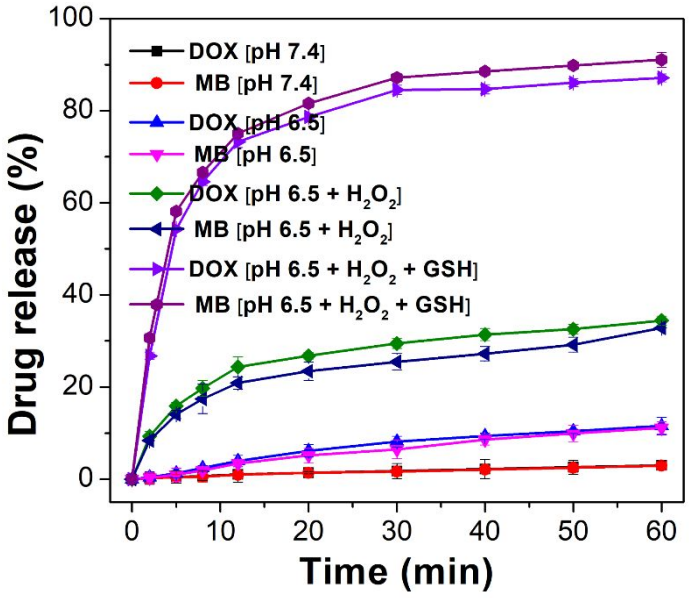

Figure S20. Released drugs from y-UCM/M&D-PEG over time in different conditions (n = 3).

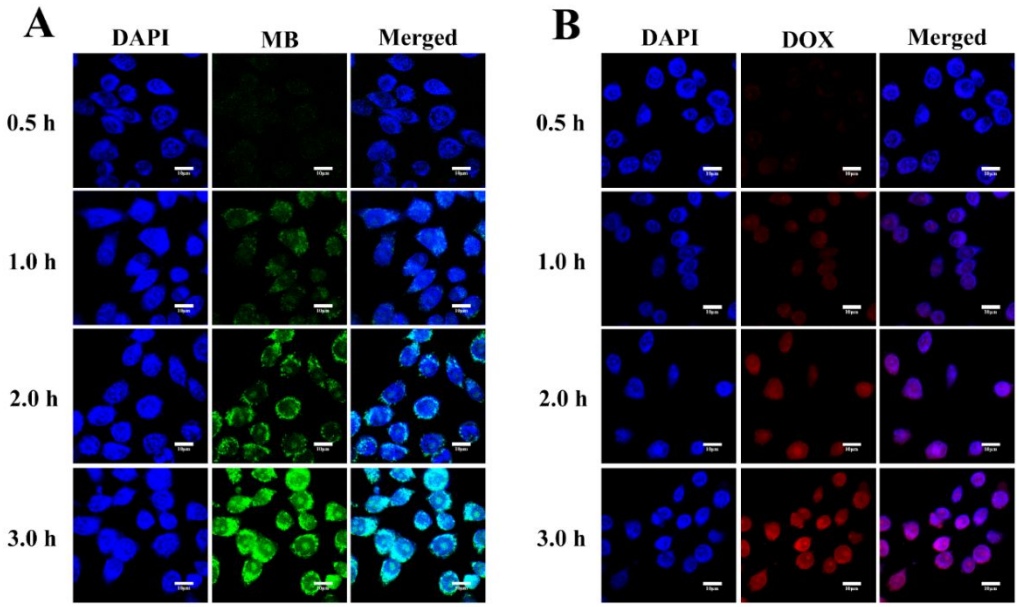

Figure S21. Confocal images of Hela cells treated with MB (A) and DOX (B) at different times points. Blue, green and red represent DAPI, MB and DOX fluorescence, respectively.

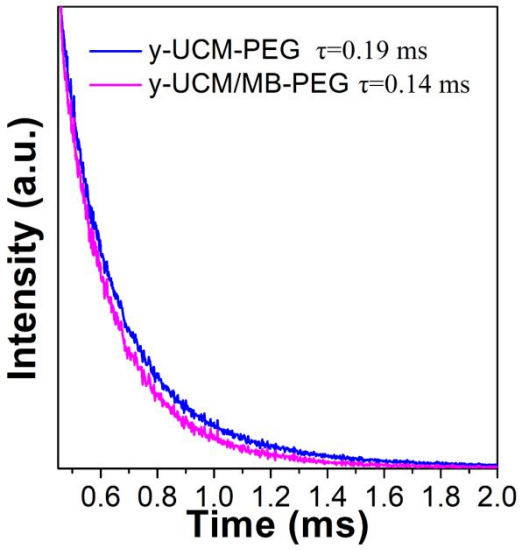

Figure S22. Lifetime decay curves at 656 nm of y-UCM-PEG and y-UCM/MB-PEG upon 980 nm laser excitation.

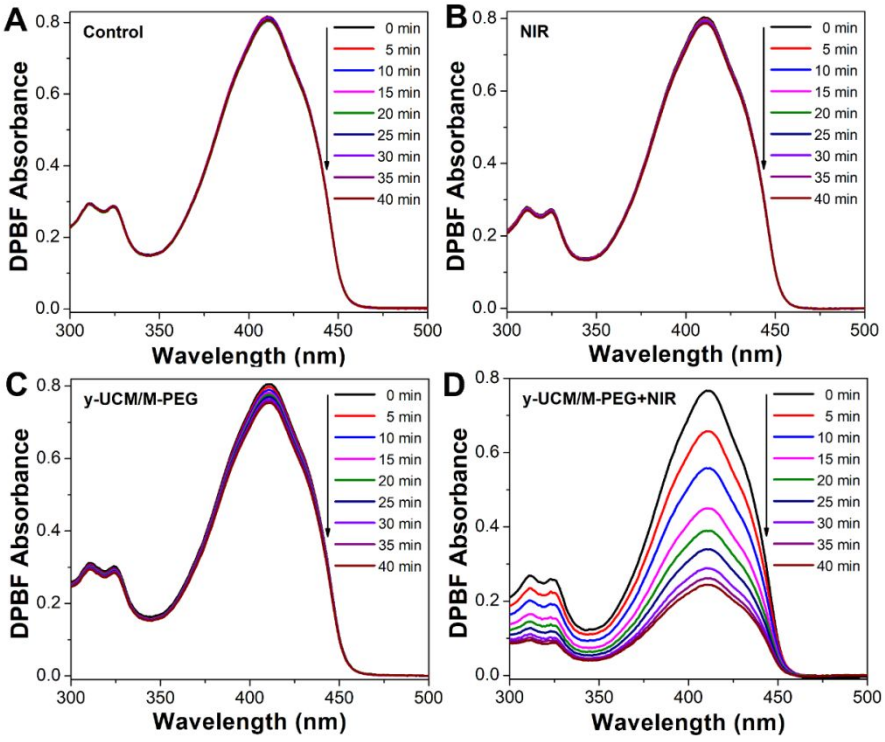

Figure S23. The variation trends of the absorbance of DPBF over time in different conditions: (A) Control, (B) NIR, (C) y-UCM/M-PEG and (D) y-UCM/M-PEG + NIR. NIR: Ex = 980 nm, 0.5 $W \cdot cm^{-2}$.

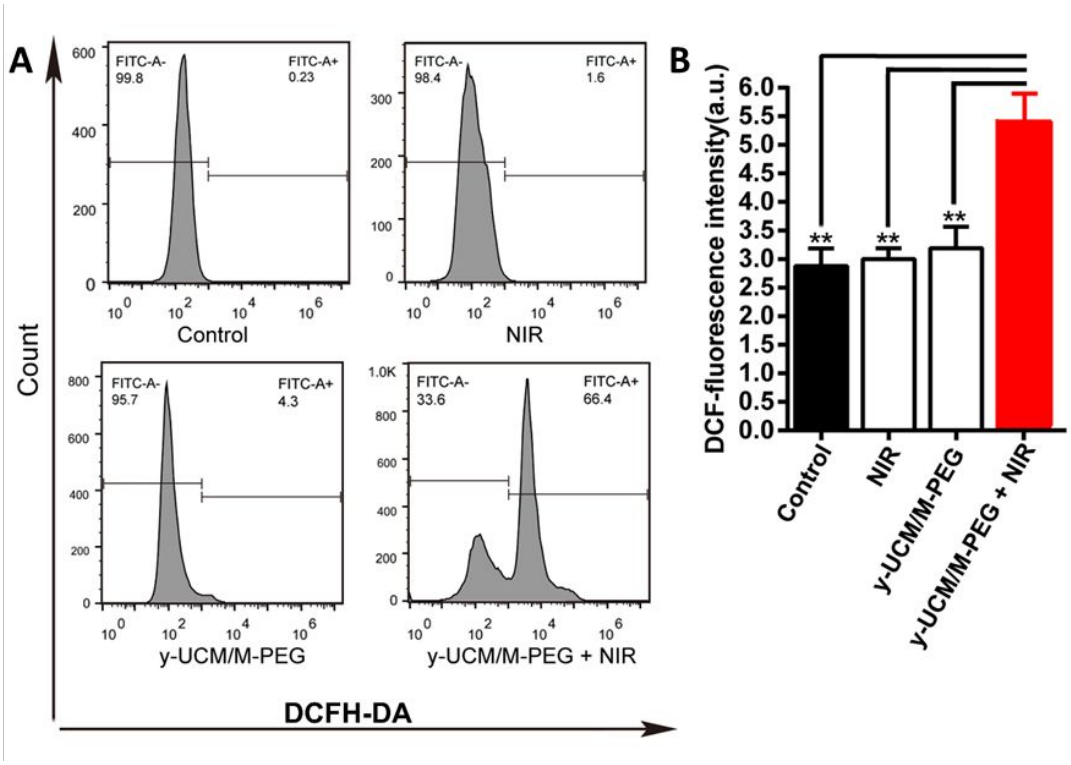

Figure S24. (A) CFSE-based flow cytometry of HeLa cells incubated with DCFH-DA and (B) DCF-fluorescence intensity in different conditions (Control, NIR, y-UCM/M-PEG and y-UCM/M-PEG+NIR, respectively). **P < 0.01 analyzed by one-way analysis of variance (ANOVA). Data represent mean ± SD (n = 3).

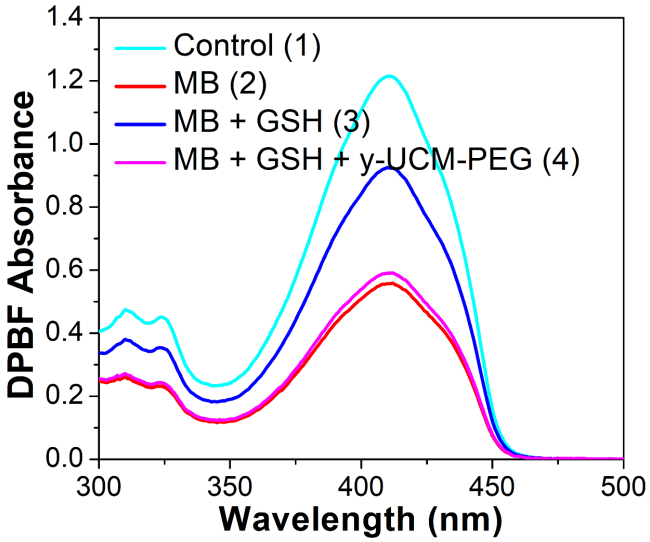

Figure S25. The DPBF absorbance in different conditions: (1) Control, (2) MB, (3) MB + GSH and (4) MB + GSH + y-UCM-PEG. 633-nm laser, 100 mW·cm^{-2}, 10 min.

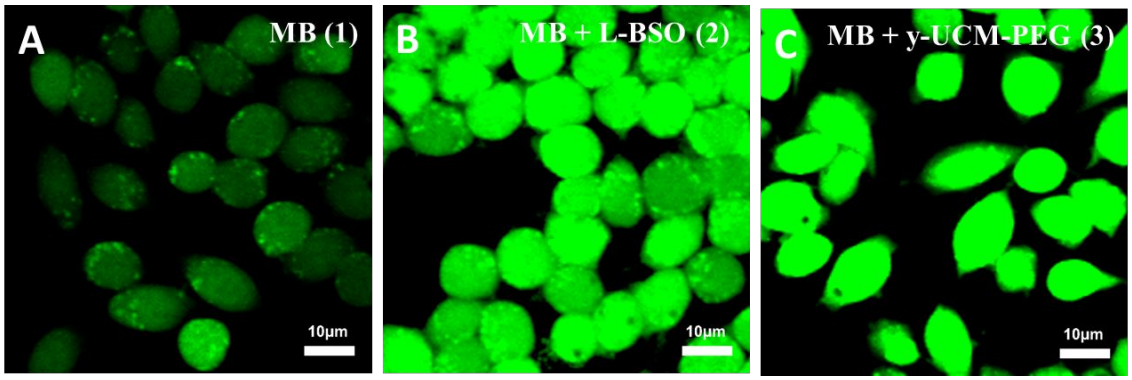

Figure S26. The effects of excessive GSH on ROS in Hela cells. Confocal images of Hela cells (A) incubated with MB, (B) pretreated with L-BSO (GSH inhibitor) for 12 h followed by incubation with MB, (C) incubated with MB + y-UCM-PEG. Fluorescence comes from DCFH-DA, Ex = 488 nm; Em = 550 ± 40 nm.

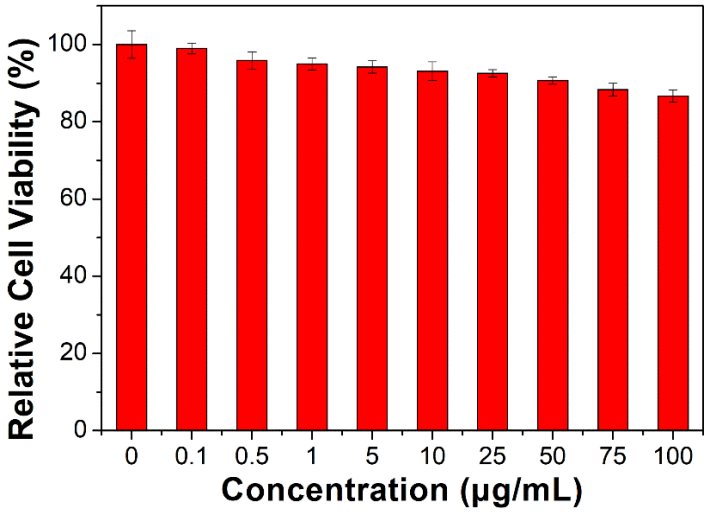

Figure S27. Relative viabilities of Hela cells after incubation with various concentrations of y-UCM-PEG in the dark for 24 h. Date are presented as means ± s.d. (n = 5).

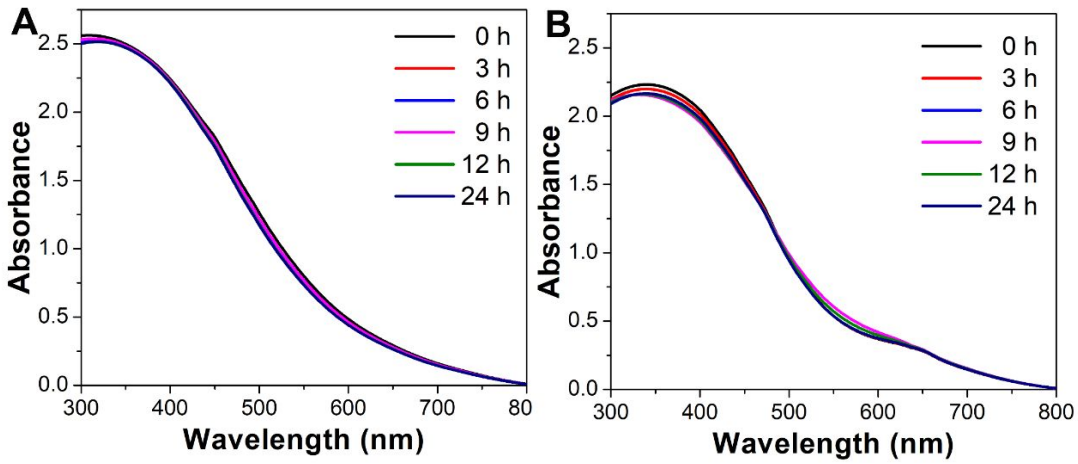

Figure S28. (A) The UV-vis absorbance spectra of y-UCM-PEG solutions in PBS (pH 7.4) and (B) DMEM (with 10% serum) after one-day standing.

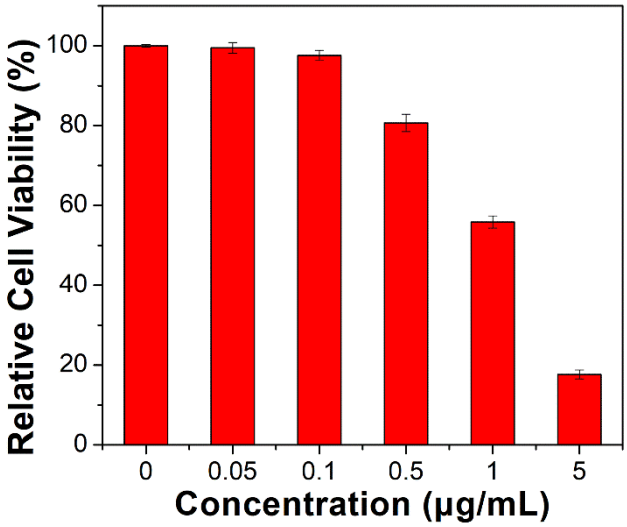

Figure S29. Relative viabilities of Hela cells after incubation with various concentrations of DOX in the dark for 24 h. Date are presented as means ± s.d. (n = 5).

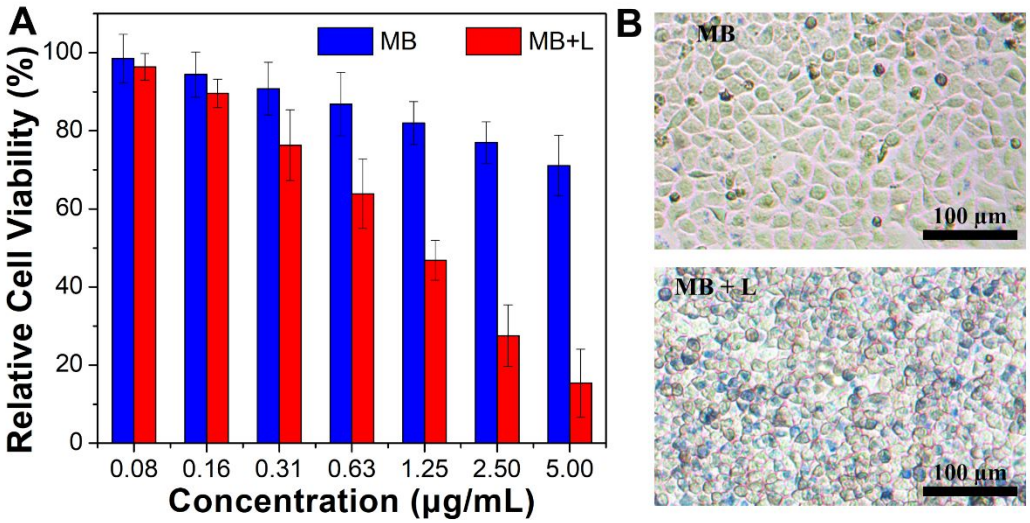

Figure S30. (A) Relative viabilities and (B) microscope images of Hela cells dyed with trypan blue after incubation with MB and MB + L. (Ex = 633 nm, 0.5 W·cm^{-2}, 5 min). Data are presented as means ± s.d. (n = 5).

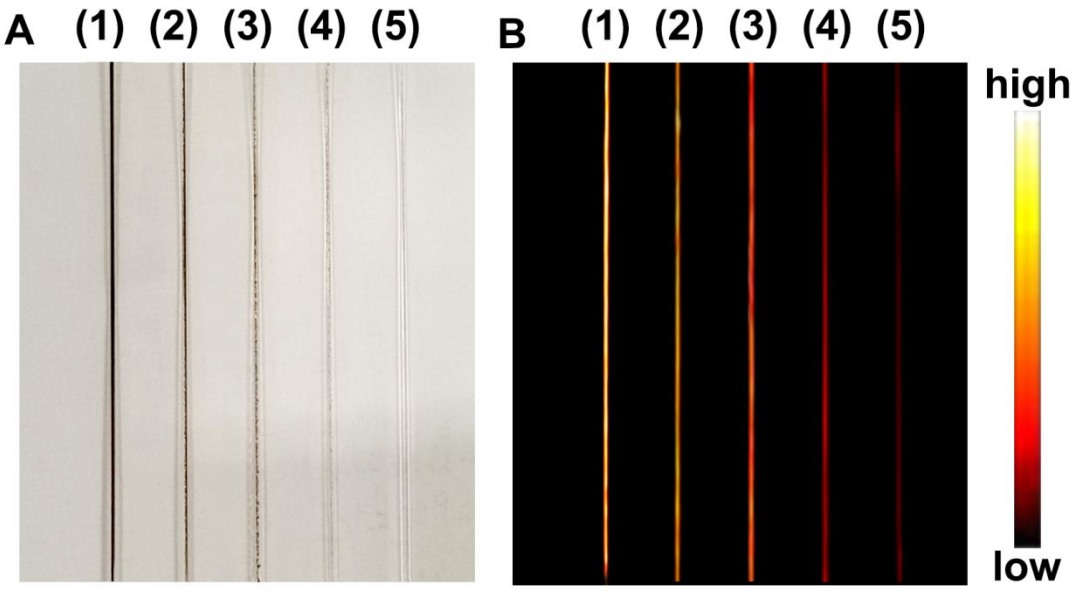

Figure S31. (A) Bright field and (B) NIR-II imaging of various concentrations of y-UCM/M&D-PEG *in vitro*. Capillary 1-5: 0.1, 0.05, 0.025, 0.013, 0.006 mM, respectively. Excitation: 980 nm (0.5 W/cm^2), exposure time: 100 ms, 1200 nm long-pass filter.

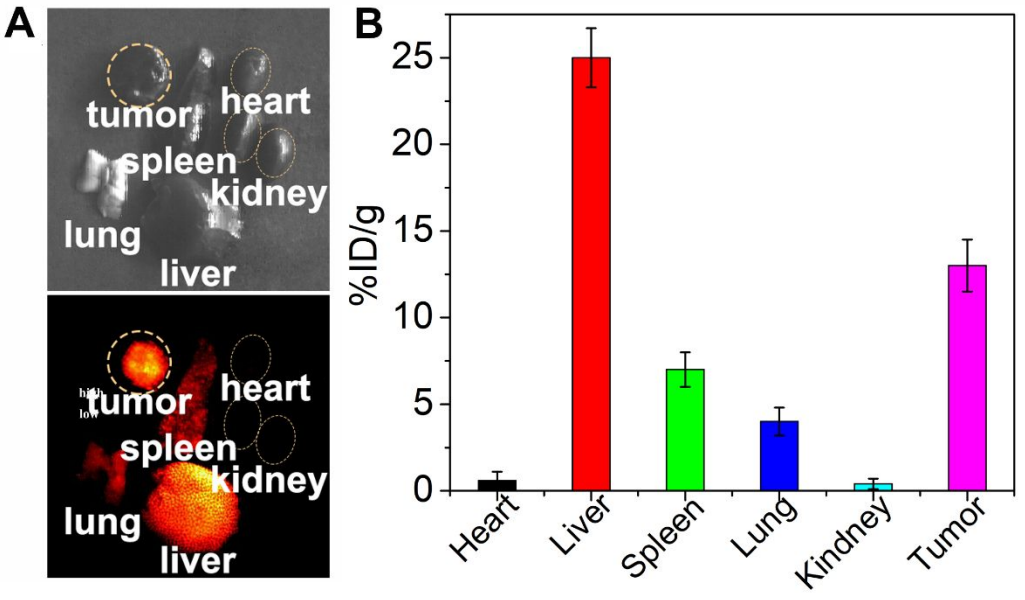

Figure S32. (A) *Ex vivo* imaging of related organs and tumor (above, bright field; bottom, fluorescence, Ex = 980 nm), and (B) the biodistribution of y-UCM/M&D-PEG in related organs and tumor at 18 h after the injection, mean ± s.d. n = 3.

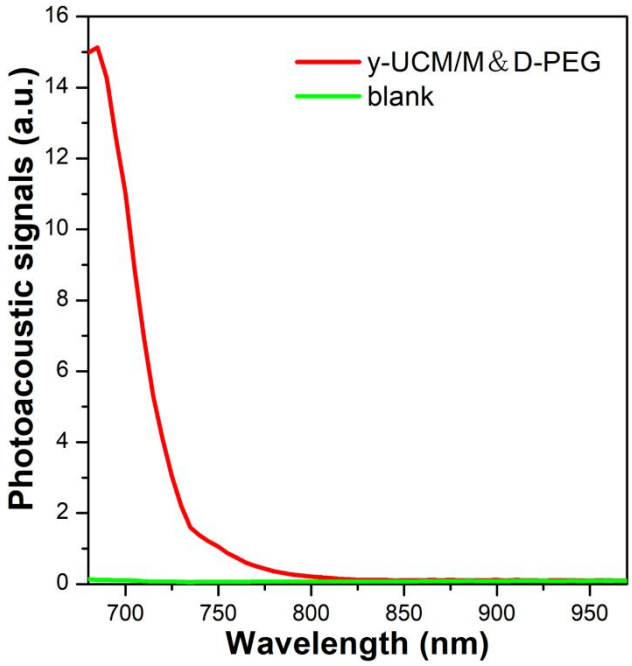

Figure S33. *In vitro* PA signals of y-UCM/M & D-PEG and H_2O versus various excitation wavelengths (680-970 nm).

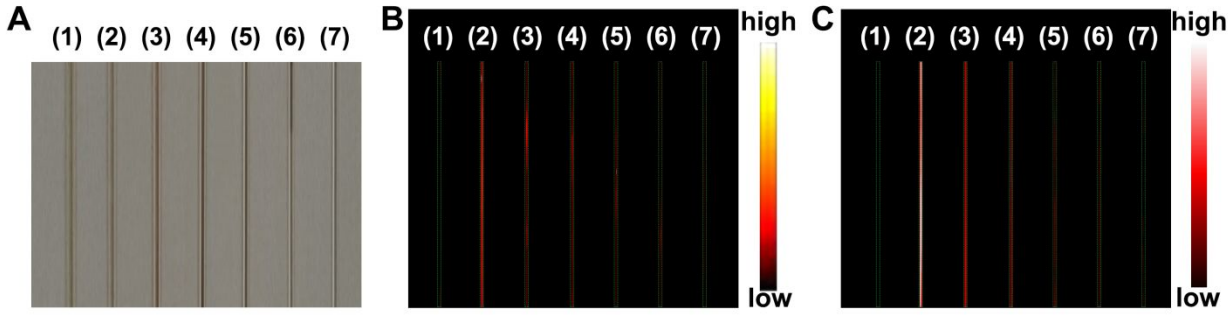

Figure S34. (A) Bright field, (B) NIR-II imaging and (C) PA imaging of blood after removal of red blood cells at different times *in vitro*. Capillary 1-7: control, 3, 6, 12, 18, 24 and 36 h, respectively. Excitation: 980 nm (0.5 W/cm^2), exposure time: 100 ms, 1200 nm long-pass filter.

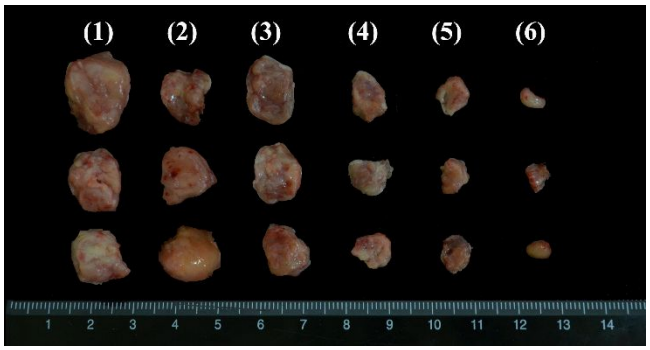

Figure S35. At the end of the entire therapeutic evaluation, photos of tumors in different groups after 15 days of treatment. (1) Untreated; (2) NIR; (3) y-UCM-PEG; (4) chemo group: y-UCM/M&D-PEG; (5) PDT group: y-UCM/M-PEG+NIR; (6) chemo-PDT combination therapy group: y-UCM/M&D-PEG+NIR. NIR: Ex = 980 nm, 0.5 W·cm^{-2}, 5 min.

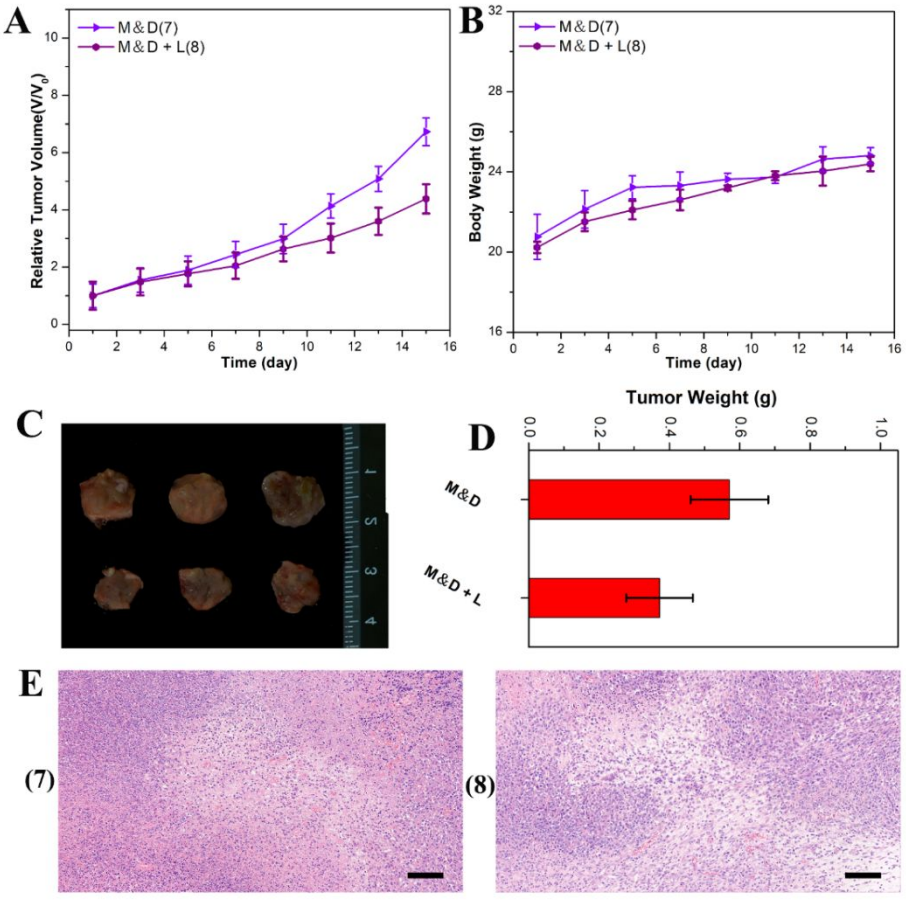

Figure S36. (A) Relative tumor volume and (B) body weight of mice in different groups during treatment. (C) Photos of tumors in different groups after 15 days of treatment. (D) Growth curves of Hela tumor-bearing nude mice after different treatments. (E) Histopathological analysis of tumors after different treatments. (7): MB; (8): MB + L (Ex = 633 nm, 0.5 W·cm^{-2}, 5 min).

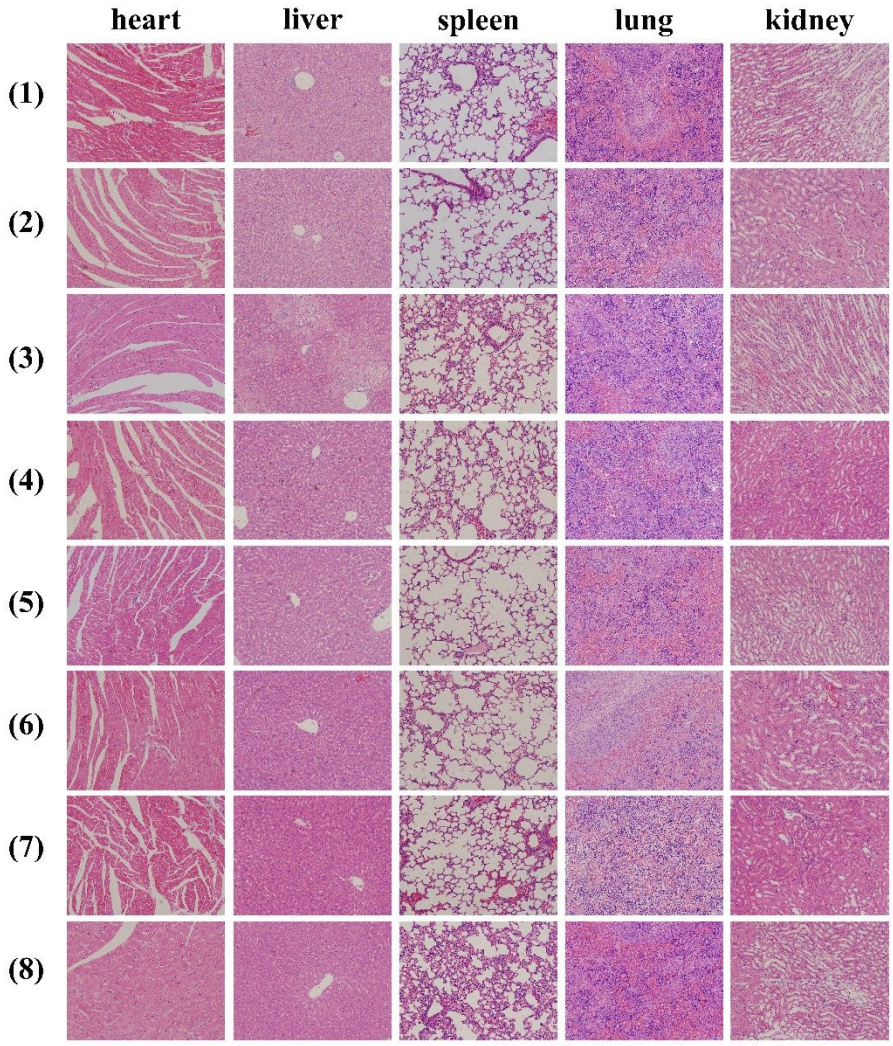

Figure S37. Histopathological analysis of heart, liver, spleen, lung and kidney after different treatments.

(1): saline; (2): NIR; (3): y-UCM-PEG; (4): y-UCM/M&D-PEG; (5): y-UCM/M-PEG+NIR (Ex = 980 nm, 0.5 W·cm^{-2}, 5 min); (6): y-UCM/M&D-PEG+NIR (Ex = 980 nm, 0.5 W·cm^{-2}, 5 min); (7): MB; (8): MB + L (Ex = 633 nm, 0.5 W·cm^{-2}, 5 min).

3. Additional Tables

Table S1. Blood biochemistry and hematology data of female mice

Project Name	Control Group Mean ± SD	Treatment Group Mean ± SD
ALT(U/L)	36.45 ±2.74	36.02 ±3.42
AST(U/L)	148.47 ±8.17	148.09 ±5.59
ALB(g/L)	22.46 ±2.95	22.27 ±2.83
A/G	0.40 ±0.02	0.40 ±0.02
BUN(mmol/L)	5.90 ±0.63	5.87 ±0.31
HCT(%)	43.97 ±0.71	43.51 ±0.42
HGB(g/L)	158.22±4.82	158.40 ±1.93
MCH(pg)	10.83 ±1.23	10.97 ±0.56
MCHC(g/L)	342.28 ±6.69	341.10 ±4.23
MCV(fL)	41.13 ±0.86	41.31 ±0.75
MPV(fL)	7.01 ±0.08	7.04 ±0.12
PLT(10^{11}/L)	9.64 ±0.34	9.65 ±0.28
RBC(10^{12}/L)	9.83 ±0.41	9.89 ±0.51
WBC(10^{9}/L)	8.12 ±0.03	8.13 ±0.06

Notice: the data in the table is average calculated by three mice in each group.

Healthy balb/c mice in 2 weeks of intravenous injection with y-UCM-PEG were sacrificed at 2 weeks for blood collection. Serum biochemistry data including alanine aminotransferase (ALT), aspartate aminotransferase (AST), albumin (ALB), the ratio of albumin and globulin (A/G), blood urea nitrogen (BUN) levels, hematocrit (HCT), hemoglobin (HGB), mean corpuscular haemoglobin (MCH), mean corpuscular hemoglobin concentration (MCHC), mean corpuscular volume (MCV), mean platelet volume (MPV), platelets (PLT), red blood cells (RBC) and white blood cells (WBC).

4. References

(1) Wang, F.; Deng, R. R.; Liu, X. G. Preparation of Core-Shell $NaGdF_4$ Nanoparticles Doped with Luminescent Lanthanide Ions to Be Used as Upconversion-Based Probes. *Nature Protocols* **2014,** *9*, 1634-1644.

(2) Li, X. M.; Shen, D. K.; Yang, J. P.; Yao, C.; Che, R. C.; Zhang, F.; Zhao, D. Y. Successive Layer-by-Layer Strategy for Multi-Shell Epitaxial Growth: Shell Thickness and Doping Position Dependence in Upconverting Optical Properties. *Chem. Mater.* **2013,** *25*, 106-112.

(3) Li, X. M.; Zhou, L.; Wei, Y.; El-Toni, A. M.; Zhang, F.; Zhao, D. Y. Anisotropic Growth-Induced Synthesis of Dual-Compartment Janus Mesoporous Silica Nanoparticles for Bimodal Triggered Drugs Delivery. *J. Am. Chem. Soc.* **2014,** *136*, 15086-15092.

(4) Yang, G. B.; Xu, L. G.; Chao, Y.; Xu, J.; Sun, X. Q.; Wu, Y. F.; Peng, R.; Liu, Z. Hollow MnO_2 as a Yumor-Microenvironment-Responsive Biodegradable Nano-platform for Combination Therapy Favoring Antitumor Imune Responses. *Nat. Commun.* **2017,** *8*, 902.